VOL. 4, NO. 10, DECEMBER 2009 ISSN 1819-6608
ARPN Journal of Engineering and Applied Sciences


www.arpnjournals.com

# THE CHARACTERISTICS OF BRAZED PLATE HEAT EXCHANGERS WITH DIFFERENT CHEVRON ANGLES

M. Amala Justus Selvam[1], Senthil kumar P.[2] and S. Muthuraman[3]
[1]Sathyabama University, Tamil Nadu, India
[2]K. S. R College of Engineering, Tamil Nadu, India
[3]Sun College of Engineering and Technology, Tamil Nadu, India
E-Mail: muthu9678@rediffmail.com

**ABSTRACT**

Experiments to measure the condensation heat transfer coefficient and the pressure drop in brazed plate heat exchangers (BPHEs) were performed with the refrigerants R410A and R22. Brazed plate heat exchangers with different chevron angles of 45°, 35°, and 20° were used. Varying the mass flux, the condensation temperature, and the vapor quality of the refrigerant, we measured the condensation heat transfer coefficient and the pressure drops. Both the heat transfer coefficient and the pressure drop increased proportionally with the mass flux and the vapor quality and inversely with the condensation temperature and the chevron angle. Correlations of the Nusselt number and the friction factor with the geometric parameters are suggested for the tested BPHEs.

**Keywords**: condensation, brazed plate heat exchanger, r410a, chevron angle, correlation.

## 1. INTRODUCTION

Plate heat exchangers (PHEs) were introduced in the 1930s and were almost exclusively used as liquid/liquid heat exchangers in the food industries because of their ease of cleaning. Over the years, the development of the PHE has generally continued towards larger capacity, as well as higher working temperature and pressure. Recently, a gasket sealing was replaced by a brazed material, and each thermal plate was formed with a series of corrugations (herringbone or chevron). These greatly increased the pressure and the temperature capabilities.

The corrugated pattern on the thermal plate induces a highly turbulent fluid flow. The high turbulence in the PHE leads to an enhanced heat transfer, to a low fouling rate, and to a reduced heat transfer area. Therefore, PHEs can be used as alternatives to shell-and-tube heat exchangers. Due to ozone depletion, the refrigerant R22 is being replaced by R410A (a binary mixture of R32 and R125, mass fraction 50 %/50 %). R410A approximates an azeotropic behavior since it can be regarded as a pure substance because of the negligible temperature gliding. The heat transfer and the pressure drop characteristics in PHEs are related to the hydraulic diameter, the increased heat transfer area, the number of the flow channels, and the profile of the corrugation waviness, such as the inclination angle, the corrugation amplitude, and the corrugation wavelength. These geometric factors influence the separation, the boundary layer, and the vortex or swirl flow generation. However, earlier experimental and numerical works were restricted to a single-phase flow. Since the advent of a Brazed PHE (BPHE) in the 1990s, studies of the condensation and/or evaporation heat transfer have focused on their applications in refrigerating and air conditioning systems, but only a few studies have been done. Much work is needed to understand the features of the two-phase flow in the BPHEs with alternative refrigerants. Xiaoyang *et al*., [1] experimented with the two-phase flow distribution in stacked PHEs at both vertical upward and downward flow orientations. They indicated that non-uniform distributions were found and that the flow distribution was strongly affected by the total inlet flow rate, the vapor quality, the flow channel orientation, and the geometry of the inlet port Holger [2].

Theoretically predicted the performance of chevron-type PHEs under single-phase conditions and recommended the correlations for the friction factors and heat transfer coefficients as functions of the corrugation chevron angles. Lee *et al*., [3] investigated the characteristics of the evaporation heat transfer and pressure drop in BPHEs with R404A and R407C. Kedzierski [4] reported the effect of inclination on the performance of a BPHE using R22 in both the condenser and the evaporator. Several single-phase correlations for heat transfer coefficients and friction factors have been proposed, but few correlations for the two-phase flow have been proposed. Yan *et al*., [5] suggested a correlation of condensation with a chevron angle of 30 for R134a. Yan *et al*., reported that the mass flux, the vapor quality, and the condensation pressure affected the heat transfer coefficients and the pressure drops. Hieh and Lin [6] developed the correlations for evaporation with a chevron angle of 30 for R410A.

The main objective of this work was to experimentally investigate the heat transfer coefficients and the pressure drops during condensation of R410A inside BPHEs. Three BPHEs with different chevron angles of 45, 35, and 20 were used. The results were then compared to those of R22. The geometric effects of the plate on the heat transfer and the pressure drop were investigated by varying the mass flux, the quality, and the condensation temperature. From the results, the geometric effects, especially the chevron angle, must be considered to develop the correlations for the Nusselt number and the friction factor. Correlations for the Nusselt number and the

friction factor with the geometric parameters are suggested in this study.

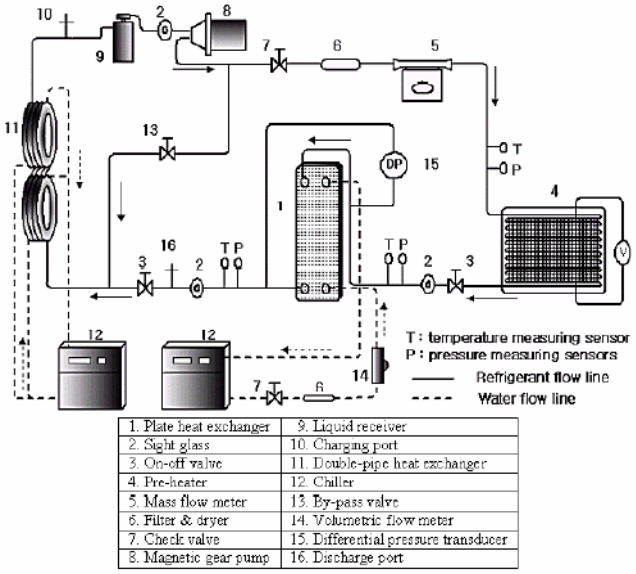


| | |
|---|---|
| 1. Plate heat exchanger | 9. Liquid receiver |
| 2. Sight glass | 10. Charging port |
| 3. On-off valve | 11. Double-pipe heat exchanger |
| 4. Pre-heater | 12. Chiller |
| 5. Mass flow meter | 13. By-pass valve |
| 6. Filter & dryer | 14. Volumetric flow meter |
| 7. Check valve | 15. Differential pressure transducer |
| 8. Magnetic gear pump | 16. Discharge port |

Fig. 1. Schematic diagram of the experimental system.

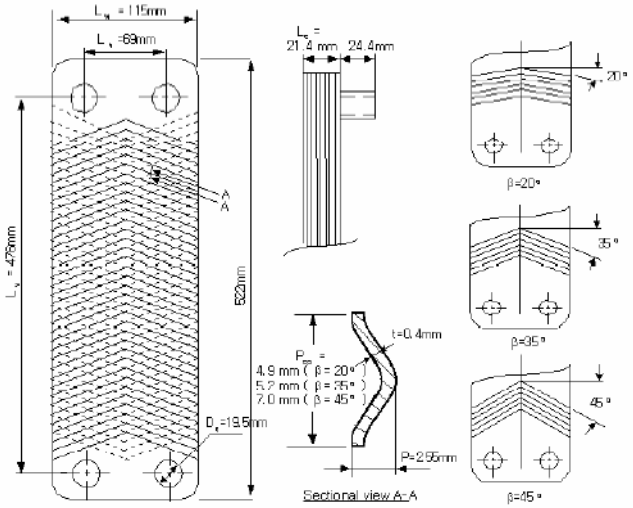


Fig. 2. Dimensions of the brazed plate heat exchangers.

## 2. EXPERIMENTAL FACILITY

The experimental facility is capable of determining in plate heat transfer coefficients and measuring the pressure drops for the refrigerants. It consists of four main parts: a test section, a refrigerant loop, two water loops, and a data-acquisition system. A schematic of the test facility used in this study is shown in Figure-1, and detailed descriptions of the four main parts are mentioned below.

### 2.1 Brazed plate heat exchangers

Three BPHEs with chevron angles of 45°, 35°, and 20° were used as the test sections. The angles of corrugation were measured from the horizontal axis. Each BPHE was composed of 4 thermal plates and 2 end plates, forming 5 flow channels. The dimensions of the BPHEs are shown in Figure-2. The refrigerant and cooling water were directed into the alternate passages between the plates through corner ports, creating counter flow conditions. The cooling water owed from the bottom to the top of every other channel on the basis of a central channel. On the other hand, the refrigerant owed from the top to the bottom in the rest of them.

### 2.2 Refrigerant loop

Refrigerant was supplied to the test section at specific conditions (i.e., temperature, flow rate, and quality) through the refrigerant loop. This loop contained a pre-heater, a double-pipe heat exchanger, a receiver, a magnetic gear pump, a differential pressure transducer, and a mass flow meter. Also included were thermocouples probes and pressure taps at the inlet/outlet of the test section. The refrigerant pump was driven by a DC motor which was controlled by a variable DC output motor controller.

The refrigerant flow rate was measured by using a mass flow meter installed between the magnetic gear pump and the pre-heater with an accuracy of _0.5 %. The pre-heater located before the test section was used to evaporate the refrigerant to a specified vapor quality at the inlet of the test section. The pressure drop of the refrigerant owing through the test section was measured with the differential pressure transducer, to an accuracy of _0.25 kPa. The refrigerant through the test section was subcooled at a double-pipe heat exchanger by the water cooled by the chiller and went into a liquid receiver. The subcooled refrigerant returned to the magnetic gear pump and circulated through the refrigerant loop repeatedly. Calibrated T-type thermocouples were used to measure the temperatures of the refrigerant at the inlet/outlet of the test section. The entire loop was insulated with fiberglass to prevent heat transfer to the environment.

### 2.3 Water loop

There are two closed water loops in this facility. One is for determining the condensation heat flux at the test section. The other is for making the subcooled refrigerant state at two double-pipe heat exchangers before it enters the magnetic gear pump. The water flow rates of the test section were measured by using a turbine flow meter, and T-type thermocouples were installed to evaluate the gain of the heat flux of the water of the test section.

### 2.4 Data acquisition

The data were recorded by a computer-controlled data-acquisition system with 40 channels scanned at the speed of 30 data per minute. The temperature and the pressure of both fluids were continuously recorded, and the thermodynamic properties of the refrigerant were

obtained from a computer program. After steady-state conditions had been reached in the system, all measurements were taken for 10 minutes.

## 3. DATA REDUCTION AND UNCERTAINTY ANALYSIS

The hydraulic diameter of the channel, DH, is defined as

$$D_h = \frac{4 \times \text{channel flow area}}{\text{wetted perimeter}} = \frac{4bL_w}{2L_w\phi} = \frac{2b}{\phi}, \quad (1)$$

Where φ is 1.17. This value is given by the manufacturer. The mean channel spacing, b, is defined as

**b = p - t;** (2)

and the plate pitch p can be determined as

$$p = \frac{L_c}{N_t - 1}. \quad (3)$$

The procedures to calculate the condensation heat transfer coefficient of the refrigerant side are described below. At first, the refrigerant quality at the inlet of the test section (xin) should be selected to evaluate the condensation heat at a given quality. Its value is calculated from the amount of heat given by a pre-heater, which is the summation of the sensible heat and the latent heat:

$$Q_{pre} = Q_{sens} + Q_{lat} = \dot{m}_r C_{p,r}(T_{r,sat} - T_{r,pre,in}) + \dot{m}_r i_{fg} x_{in}. \quad (4)$$

The refrigerant quality at the inlet of the test section can be written as

$$x_{in} = \frac{1}{i_{fg}} \left[ \frac{Q_{pre}}{\dot{m}_r} - C_{p,r}(T_{r,sat} - T_{r,pre,in}) \right]. \quad (5)$$

The power gained by the pre-heater is calculated by measuring the voltage and the current with a power meter. The change in the refrigerant quality inside the test section was evaluated from the heat transferred in the test section and the refrigerant mass flow rate (6)

$$\Delta x = x_{in} - x_{out} = \frac{Q_w}{\dot{m}_r \times i_{fg}}. \quad (6)$$

The condensing heat in the test section was calculated from an energy balance with water:

$$Q_w = \dot{m}_w C_{p,w}(T_{w,out} - T_{w,in}). \quad (7)$$

The heat transfer coefficient of the refrigerant side (hr) was evaluated from the following equation:

$$\frac{1}{h_r} = \frac{1}{U} - \frac{1}{h_w} - R_{wall}. \quad (8)$$

The overall heat transfer coefficient was determined using the log mean temperature difference

$$U = \frac{Q_w}{A \times LMTD},$$
$$LMTD = \frac{(T_{r,out} - T_{w,in}) - (T_{r,in} - T_{w,out})}{\ln\{(T_{r,out} - T_{w,in})/(T_{r,in} - T_{w,out})\}}. \quad (9)$$

The heat transfer coefficient of the water side (HW) was obtained by using Eq. (10). Equation (10) was developed from the single-phase water to water pre-tests by Kim [7]. If the least-squares method and the multiple regression method are used, the heat transfer coefficient of the water side is correlated in terms of the Reynolds number, the Prandtl number, and the chevron angle:

$$h_w = 0.295 \left( \frac{k_w}{D_{Eq}} \right) Re^{0.64} Pr^{0.32} \left( \frac{\pi}{2} - \beta \right)^{0.09}. \quad (10)$$

The thermal resistance of the wall is negligible compared to the effect of convection.
For the vertical downward flow, the total pressure drop in the test section is defined as

$$\Delta P_{total} = \Delta P_{fr} + \Delta P_a + \Delta P_s + \Delta P_p, \quad (11)$$

And Ptotal is measured by using a differential pressure transducer. The two-phase friction factor, f, is defined as

$$\Delta P_{fr} = f \frac{L_v N_{cp}}{D_h} \frac{G_{Eq}^2}{\rho_f}. \quad (12)$$

The port pressure loss in this experiment was less than 1 % of the total pressure loss. The static head loss can be written as and it has a negative value for vertical downward flow. The acceleration pressure drop for condensation is expressed as

$$\Delta P_p = 1.4 G_p^2 / (2\rho_m),$$

An uncertainty analysis was done for all the measured data and the calculated quantities based on the methods described by Moffat [9]. The detailed results of the uncertainty analysis are shown in Table-1.

Table 1. Estimated uncertainty.

| Parameters | Uncertainty |
|---|---|
| Temperature | ±0.2 °C |
| Pressure | ±4.7 kPa |
| Pressure drop | ±250 Pa |
| Water flow rate | ±2 % |
| Refrigerant mass flux | ±0.5 % |
| Heat flux of test section | ±5.7 % |
| Vapor quality | ±0.03 |
| Heat transfer coefficients of water side | ±10.1 % |
| Heat transfer coefficients of refrigerant | ±9.1 % |

where

$$G_p = 4\dot{m}_{Eq}/\pi D_p^2 \quad (14)$$

and

$$(1/\rho_m) = (x/\rho_g) + [(1-x)/\rho_f]. \quad (15)$$

The equivalent mass flow rate, $\dot{m}_{Eq}$, is defined as

$$\dot{m}_{Eq} = \dot{m}\left[1 - x + x\left(\frac{\rho_f}{\rho_g}\right)^{0.5}\right]. \quad (16)$$

The port pressure loss in this experiment was less than 1 % of the total pressure loss. The static head loss can be written as

$$\Delta P_s = -\rho_m g L_v \quad (17)$$

and it has a negative value for vertical downward flow. The acceleration pressure drop for condensation is expressed as

$$\Delta P_a = -\left[(G_{Eq}^2 x/\rho_{fg})_{in} - (G_{Eq}^2 x/\rho_{fg})_{out}\right]. \quad (18)$$

## 4. RESULTS AND DISCUSSIONS

The condensation heat transfer coefficients and the pressure drops of R410A and R22 were measured in three BPHEs with chevron angles of 20°, 35°, and 45° by varying the mass flux (13-34 kg/m$^2$s), the vapor quality (0.9-0.15), and the condensing temperature (20°C and 30°C) under a given heat flux condition (4.7-5.3 kW/m$^2$). R22 was tested under identical experimental conditions for comparison with R410A.

### 4.1 Flow regime

Before the behaviors of heat transfer are considered, it is necessary to predict what flow regime exists at a given set of operating conditions. The detailed flow regime map for the PHE has not been proposed yet because of the difficulty of flow visualization. Vlasogiannis *et al*., [10] suggested the criterion of a two-phase flow regime for a PHE in terms of superficial liquid (jf) and vapor velocities (jg) by using water and air under adiabatic conditions. They only simulated a mixture of water and air as a two-phase fluid. According to their work, the flow patterns in a PHE are significantly different from those inside the vertical round tubes. They detected 3 types of flow patterns. The first was a gas continuous pattern with a liquid pocket at flow water flow rates (jf < 0.025 m/s) over wide range of air flow rates. The second was the slug flow pattern, which was detected at sufficiently high air (jg > 2 m/s) and water flow rates (jf > 0.025 m/s). Thirdly, the liquid continuous pattern with a gas pocket or a gas bubble at the high water flow rates (jf >0.1 m/s) and low air flow rates (jg < 1 m/s).According to the flow regime map proposed by Vlasogiannis *et al*., the expected flow pattern in this experimental study is the gas continuous flow pattern with liquid pockets. However, their flow regime map has a significant limitation for use since many important features, such as the phase-change, the heating or cooling conditions, the densities or specific volumes of the working fluids, the geometries of the PHEs, etc., were not considered in detail. According to the flow regime map proposed by Crawford *et al.* [11], which was developed for vertical downward flow in a round tube, all experimental flow patterns are located in the intermittent flow regime, but this flow regime can not represent the correct flow regime in a BPHE due to the different geometries.

### 4.2 Condensation heat transfer

Figure-3 shows the effects of the refrigerant mass flux, the chevron angle, and the condensation temperature on the averaged heat transfer coefficient for R410A. The term "averaged heat transfer coefficient" means the average of the heat transfer coefficients calculated by varying the quality of the refrigerant from 0.15 to 0.9, and the coefficients were obtained from Eq. (19):

$$h_{averged} = \frac{\Sigma h_{local} x_{local}}{\Sigma x_{local}}, \quad (19)$$

Where $h_{local}$ is the local heat transfer coefficient at the local vapor quality. The experimental results indicate that the averaged heat transfer coefficients vary proportionally with the mass flux and inversely with the chevron angles and the condensation temperature.

The small chevron angle forms narrow pitches to the flow direction, creating more abrupt changes in the velocity and the flow direction, thus increasing the effective contact length and time in a BHPE. The zigzag flow increases the heat transfer, and the turbulence created by the shape of the plate pattern is also important in addition to the turbulence created by the high flow rates. Increasing the mass flux at a given condensation temperature showed that the differences in the averaged heat transfer coefficients were significantly enlarged with decreasing chevron angle. This indicates that a PHE with the small chevron angle is more effective at a large mass flux (Gc > 25 kg/m$^2$s) than at a small mass flux.

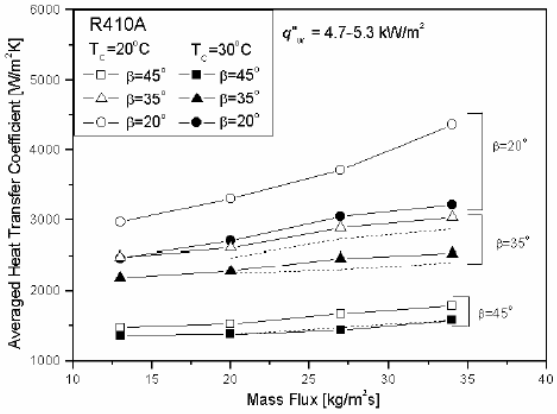


Fig. 3. Effect of mass flux on the averaged condensation heat transfer coefficient.

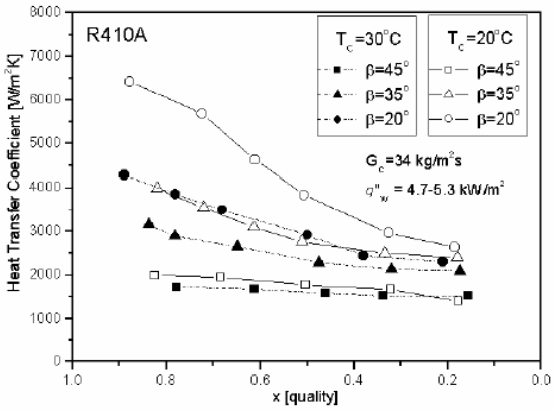


Fig. 4. Effect of quality on the condensation heat transfer coefficient.

The averaged heat transfer coefficient of R410A decreases with increasing condensation temperature. The vapor velocity is a more influential factor than the liquid film thickness for the heat transfer. Vapor bubbles in the flow enhance the disturbance in the bubble wake as a turbulence promoter, and the turbulence induced by the vapor bubbles increases with the vapor velocity. Also, since the specific volume of the vapor increases with decreasing condensation temperature, the vapor velocity increases for a fixed mass flux and quality. The vapor velocity at 20°C is faster than that at 30°C. The rates of the averaged heat transfer coefficients between condensation temperatures of 20°C and 30°C increased 5 % for a chevron angle of 45°, 9 % for 35°, and 16 % for 20°. These results show that different chevron angles lead partly to different flow pattern. Thus, we may conclude that the flow regime map should be modified by geometric considerations. The heat transfer coefficients in the high-quality region (fast velocity region) are larger than those in the low-quality region (slow velocity region). As mentioned above, this happens because the vapor velocity is the dominant effect on the heat transfer mechanism.

Increasing the vapor quality at the same mass flux induces a faster bubble velocity, which increases the turbulence level and the convection heat transfer coefficient. The difference of heat transfer coefficients between the low-quality region and the high-quality region becomes larger with decreasing chevron angle. The PHE with a low chevron angle shows a better heat transfer performance in the high-quality region (i.e., the high vapor velocity region). Figure-4 also shows the variation of the heat transfer coefficients with the condensation temperatures. Like Figure-3, the heat transfer coefficients decreased with increasing condensation temperature. Also, the variations of the heat transfer coefficients with the condensation temperature are larger in the high-quality region. From the experimental results in Figures, 3 and 4, lowering the chevron angle and the condensation temperature gives the desired heat transfer effect.

### 4.3 Frictional pressure loss

The frictional pressure loss in a BPHE is obtained by subtracting the acceleration pressure loss, the static head loss, and the port pressure loss from the total pressure loss. Figure-5 shows the trend of the pressure drop along the mass flux, and Figure-6 shows the trend of the pressure drop along the quality at a mass flux of 34 kg/m$^2$s and a heat flux of 4.7-5.3 kW/m$^2$. The frictional pressure drops in the BPHEs increase with increasing mass flux and quality and decreasing condensation temperature and chevron angle. This trend is similar to that of the condensation heat transfer. As mentioned above, since the vapor velocity is much faster than the liquid velocity during the two-phase flow in the tube, the vapor velocity is the dominant influence on the pressure drop, as well as the heat transfer. A high vapor velocity also tends to increase the turbulence of the flow. From Figures 3, 4, 5 and 6, we may concluded that since the trends of the the condensation heat transfer and the pressure loss in BPHEs are similar, those effects must be carefully considered in the design of a BPHE.

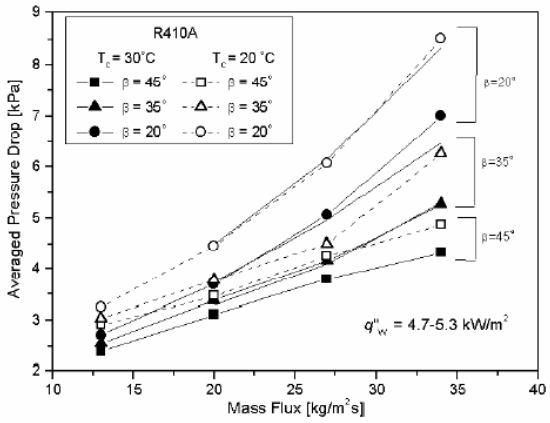


Fig. 5. Variation of the averaged condensation pressure drop with mass flux.

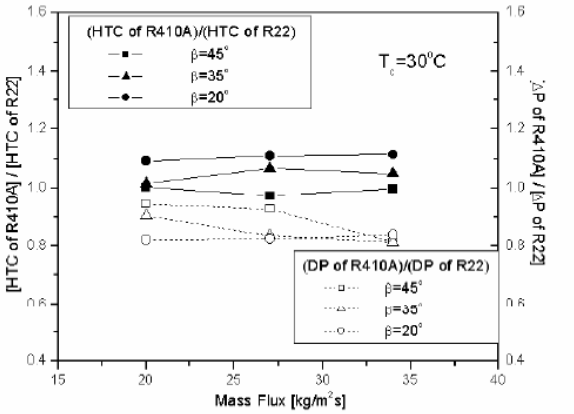


Fig. 7. Condensation heat transfer coefficient ratio and pressure drop ratio between R410A and R22.

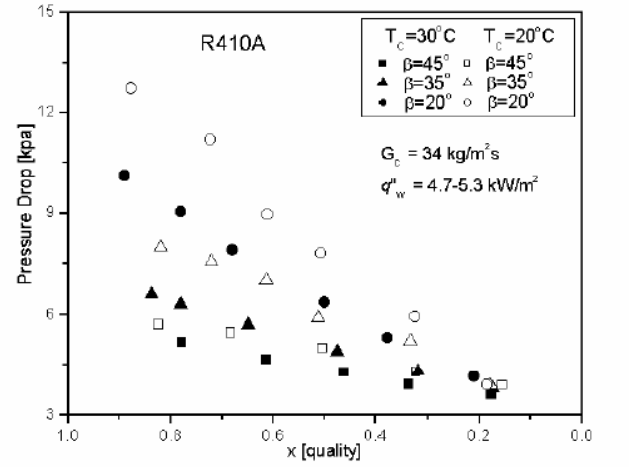


Fig. 6. Variation of the condensation pressure drop with quality.

### 4.4 Comparison of R410A with R22

The ratios of R410A to R22 for the condensation heat transfer coefficients and pressure drops at a condensation temperature of 30°C are shown in the Figure-7. The ratios for the heat transfer coefficients are relatively constant in the range of 1 -1.1, regardless of the mass flux, while the ratios for the pressure drops decrease with increasing mass flux, except for the data at a chevron angle of 20° in the present experimental range. For a chevron angle of 20°, the heat transfer ratios of R410A to R22 are about 1.1, and the pressure drop ratios about 0.8, which is a 10 % higher heat transfer and a 20 % lower pressure drop.

The smaller specific volume of the vapor of R410A relative to that of R22 makes the vapor velocity slower and yields a small pressure drop under the same conditions of the mass flux. While the two fluids have almost equal values of their latent heats, the liquid-phase thermal conductivity of R410A is larger than that of R22. The higher thermal conductivity for R410A helps to produce better heat transfer even if a reduction in the specific volume occurs. Also, a BPHE with a small chevron angle is known to have more effective performance from the ratios when replacing R22 with R410A.

### 4.5 Correlations of Nusselt number and friction factor for tested BPHEs

Based on the experimental data, the following correlations for Nu and f during condensation for the tested BPHEs are established:

$$Nu = Ge_1 Re_{Eq}^{Ge_1} Pr^{1/3}, \tag{20}$$

$$Ge_1 = 11.22 \left(\frac{p_{co}}{D_h}\right)^{-2.83} \left(\frac{\pi}{2} - \beta\right)^{-4.5}, \tag{21}$$

$$Ge_2 = 0.35 \left(\frac{p_{co}}{D_h}\right)^{0.23} \left(\frac{\pi}{2} - \beta\right)^{1.48}, \tag{22}$$

$$f = Ge_3 Re_{Eq}^{Ge_4}, \tag{23}$$

$$Ge_3 = 3521.1 \left(\frac{p_{co}}{D_h}\right)^{4.17} \left(\frac{\pi}{2} - \beta\right)^{-7.75}, \tag{24}$$

$$Ge_4 = -1.024 \left(\frac{p_{co}}{D_h}\right)^{0.0925} \left(\frac{\pi}{2} - \beta\right)^{-1.3}, \tag{25}$$

Where $G_{e1}$, $G_{e2}$, $G_{e3}$, and $G_{e4}$ are non-dimensional geometric parameters that involve the corrugation pitch, the equivalent diameter, and the chevron angle. $Re_{Eq}$ is the equivalent Reynolds number, and $G_{Eq}$ the equivalent mass flux: where $G_c$ is the channel mass flux. The suggested correlations for the Nusselt number and the friction factor can be applied in the range of $Re_{Eq}$ from 300 to 4000. Figure-8(a) shows a comparison of the Nusselt number among the experimental data, the correlation proposed in this paper, and the correlation of Yan *et al.*, [5]. The correlation of Yan *et al*., is

$$Re_{Eq} = \frac{G_{Eq} D_h}{\mu_f}, \quad (26)$$

$$G_{Eq} = G_c[1 - x + x(\rho_f/\rho_g)^{1/2}], \quad (27)$$

$$G_c = \frac{\dot{m}}{N_{cp} b L_w}, \quad (28)$$

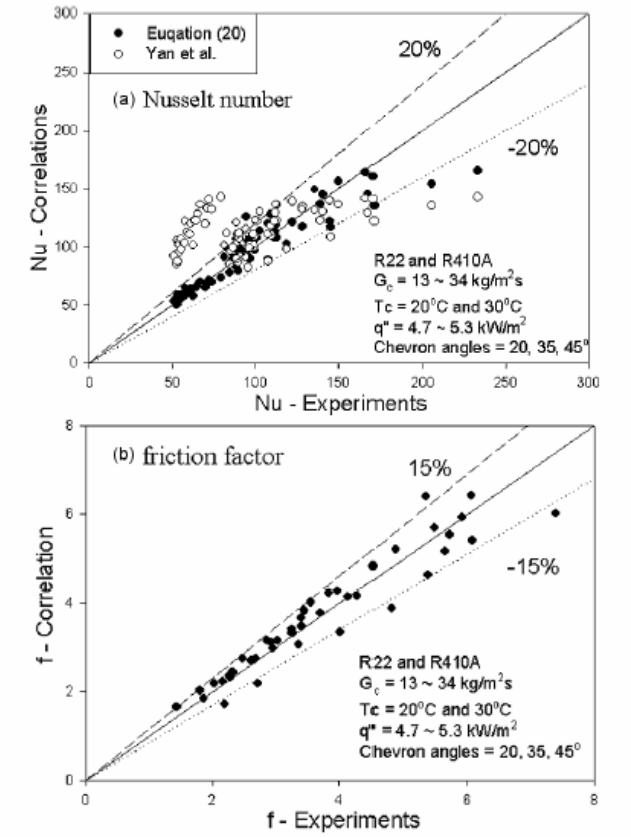


Fig. 8. Comparison of the correlations with the experimental data.

and is obtained from one PHE with a chevron angle of 30° for R134a. Regardless of the BPHE types and refrigerants, most of the experimental data are within 20 % for the correlation proposed in this paper. The correlation of Yan *et al*. (5), matched the data relatively well for $\beta$: 20 and 35 within 30 %, but over-predicted the data quite a bit for 45. This discrepancy results from the correlation of Yan *et al*., being developed for only a +30 PHE. Also, the correlation of Yan *et al*.

$$Nu = 4.118 Re_{Eq}^{0.4} Pr^{1/3}, \quad (29)$$

for the Nusselt number only adopted the equivalent Reynolds number and Prandtl number without any geometric parameters. Because a BPHE has a strong geometric effect, the correlation with geometric parameters must be developed for general applications. The root-mean-square (r.m.s.) of the deviations is defined as

$$r.m.s. = \sqrt{\frac{1}{N_{data}} \sum \left( \frac{Nu_{pred} - Nu_{\exp}}{Nu_{\exp}} \right)^2} \times 100(\%). \quad (30)$$

The r.m.s. deviation for the correlation of Yan *et al*., [Eq. (29)] is 50.2 % and for Eq. (20), it is only 10.9 %. Figure-8(b) shows a comparison of the friction factor between the experimental data and the proposed correlation. Similar to the correlation of the Nusselt number, the correlation of the friction factor includes the equivalent Reynolds number and the geometric parameters. Regardless of the BPHE types and refrigerants, most of the experimental data are within 15 % of the correlation proposed in this paper; the r.m.s. deviation for Eq. (23) is 10 %.

## 5. CONCLUSIONS

An experimental investigation has been conducted to measure the condensation heat transfer coefficient and the pressure drop of R410A and R22 in BPHEs with chevron angles of 20, 35, and 45 degrees. The experimental data were taken at two different condensation temperatures of 20°C and 30°C in the range of mass flux of 14-34 kg/m$^2$s with a heat flux of 4.7 -5.3 kW/m$^2$.

- Both the heat transfer coefficient and the pressure drop increased proportionally with the mass flux and the vapor quality and inversely with the condensation temperature and the chevron angle. Those effects must be carefully considered in the design of a BPHE due their opposing effects.
- A comparison of the data for R410A and R22 showed that the heat transfer coefficient for R410A was about 0 - 10 % larger and the pressure drop about 2- 21 % lower than those for R22. Therefore, R410A is a suitable alternative refrigerant for R22.
- Correlations for the Nusselt number and the friction factor with the geometric parameters were suggested for the tested BPHEs within 20 % (r.m.s. deviation: 10.9 %) for Nu and 15 % (r.m.s. deviation: 10 %) for f.

## APPENDIX- A

### Nomenclature

A heat transfer area of plate [m$^2$]
b mean channel spacing [m]
Cp constant pressure specific heat [J/kg K]
D diameter [m]
f friction factor
G mass flux [kg/m$^2$s]
Ge non-dimensional geometric parameter
g gravitational acceleration [m/s$^2$]
h heat transfer coefficient [W/m$^2$K]
i enthalpy [J/kg]
j superficial velocity [m/s]
Lc distance between the end plates [m]

Lh distance between the ports at the same height [m]
Lv vertical length of the fluid path between the upper and the lower ports [m]
Lw horizontal length of the plates [m]
LMTD log mean temperature difference [°C]
m mass flow rate [kg/s]
Ncp number of channels for the refrigerant
Ndata total number of data
Nt total number of plates
Nu Nusselt number
Nuexp Nusselt number obtained from experiment
Nupred Nusselt number predicted by correlation
p plate pitch [m]
pco corrugation pitch [m]
Pr Prandtl number [v]
Q heat transfer rate [W]
q heat flux [$W/m^2$]
Re Reynolds number
T temperature [°C]
t plate thickness [m]
U overall heat transfer coefficient [$W/m^2$ K]
x quality

**Subscripts**

| | |
|---|---|
| a | acceleration |
| c | channel |
| Eq | equivalent |
| f | liquid |
| fg | difference the liquid phase and the vapor phase |
| fr | friction |
| g | vapor |
| in | inlet |
| lat | latent |
| m | mean |
| out | outlet |
| p | port |
| pre | pre-heater |
| r | refrigerant |
| s | static |
| sat | saturated |
| sens | sensible |
| w | water |

**REFERENCES**

[1] R. Xiaoyang, K. Masahiro and J. G. Burgers. 1995. ASME. 225: 115.

[2] M. Holger. 1996. Chem. Eng. Proc. 35: 301.1996

[3] G. J. Lee, J. Lee C. D. Jeon and O. K. Kwon. 1999. In: Proceedings of the 1999 Summer Meeting of the SAREK, edited by C. S. Yim (SAREK, Nov.). p. 144.

[4] M. A. Kedzierski. 1997. Heat Trans. Eng. 18: 25.

[5] Y. Y. Yan, H. C. Lio and T. F. Lin. 1999. Int. J. Heat and Mass Transfer. 42: 993.

[6] Y. Y. Hsieh and T. F. Lin. 2002. Int. J. Heat and Mass Transfer. 45: 1033.

[7] Y. S. Kim. 1999. M.S. Thesis. Yonsei University.

[8] S. Kakac and H. Liu. 1998. Heat Exchangers Selection, Rating and Thermal Design. CRC Press, Boca Raton. p. 323.

[9] R. J. Mo. 1982. ASME J. Fluids Eng. 107: 173.

[10] P. Vlasogiannis, G. Karajiannis and P. Argyoropoulos. 2002. Int. J. Multiphase Flow. 28: 757.

[11] T. J. Crawford, C. B. Weinberger and J. Weisman. 1985. Int. J. Multiphase Flow. 11: 297.